Computerized classification of microcalcifications on mammograms using fuzzy logic and genetic algorithm

Yongbum Lee[*a] and Du-Yih Tsai[a]
[a]Dept. of Radiology, School of Health Sciences, Faculty of Medicine, Niigata Univ.,
2-746 Asahimachi-dori, Niigata, Niigata, Japan, 951-8518

ABSTRACT

The purpose of this study is to develop a computerized scheme for the discrimination between benign and malignant clustered microcalcifications that would aid radiologists in interpreting mammograms. In our scheme, microcalcifications in regions of interest (ROIs) are detected by using morphological filter. Then, four feature values including the total number, mean area, mean circularity and mean minimum distance of microcalcifications are calculated for classification. Gaussian-distributed membership functions used for fuzzy logic are determined from means and standard deviations of these feature values. Finally, fuzzy logic using the genetic-algorithm for optimization of membership functions is employed to classify clustered microcalcifications in unknown ROI. Our scheme was applied to twenty mammographic images with microcalcifications in the Mammographic Image Analysis Society database, containing thirteen benign and twelve malignant ROIs. Of the images ten each benign and malignant ROIs were used for training in fuzzy logic. The remaining five images were classified as benign or malignant cases by fuzzy logic. All sets of their combinations were employed to obtain the result. As the results, the average accuracy was approximately 88% (sensitivity: 100%, specificity: 77%), and Az value of ROC curve was 0.95.

Keywords: computer-aided diagnosis, microcalcification, mammogram, automated classification, fuzzy logic, genetic algorithm

INTRODUCTION

Breast cancer is a leading cause of cancer deaths among women in many parts of the world. Mammography is known as the most effective modality for early detection of breast cancer, such as tumors and microcalcifications. Detection of microcalcifications is especially related to early detection of breast cancer because those are considered to be suspicious observations in the early stages of cancer. Thus, development of computer-aided diagnosis (CAD) system is strongly desirable. In the CAD, it is important to develop a technique for not only detection of lesions but classification of them. Once the suspicious lesion has been detected in mammography, biopsy is generally executed by extracting cells around the lesion. Since it is an invasive treatment, it imposes burden of pain for patient. Therefore, it is considered that computerized classification for suspicious lesion can be helpful for decreasing unnecessary biopsy, and can assist radiologists in their diagnosis.

Some methods of classifications of microcalcifications in mammography have been reported [1-5]. In these studies, methods using neural network based on feature values of microcalcifications[1-3], and using genetic algorithm (GA) for selecting adequate features[4] have been proposed. However, it is known that a lot of information used for interpretation of medical images is fuzzy. So there have been researches on the application of fuzzy logic to the CAD in medical images [6-8].

In this paper, we propose a new scheme to classify clustered microcalcifications using fuzzy logic with genetic algorithm (GA-FL). Details of scheme and results of applying this scheme to a small number of cases are presented as well. The performance of our method is evaluated in terms of accuracy, sensitivity, specificity, and Az value of receiver-operating-characteristic (ROC) curve.

2. METHOD

2.1 Overall scheme

Our procedural flowchart is shown in Fig.1. The process consists of training phase and recognition phase. Our scheme needs regions of interest (ROIs) including microcalcifications on mammogram. In training phase, first,

Medical Imaging 2004: Image Processing, edited by J. Michael Fitzpatrick, Milan Sonka, Proceedings of SPIE Vol. 5370 (SPIE, Bellingham, WA, 2004)
1605-7422/04/$15 doi: 10.1117/12.536274

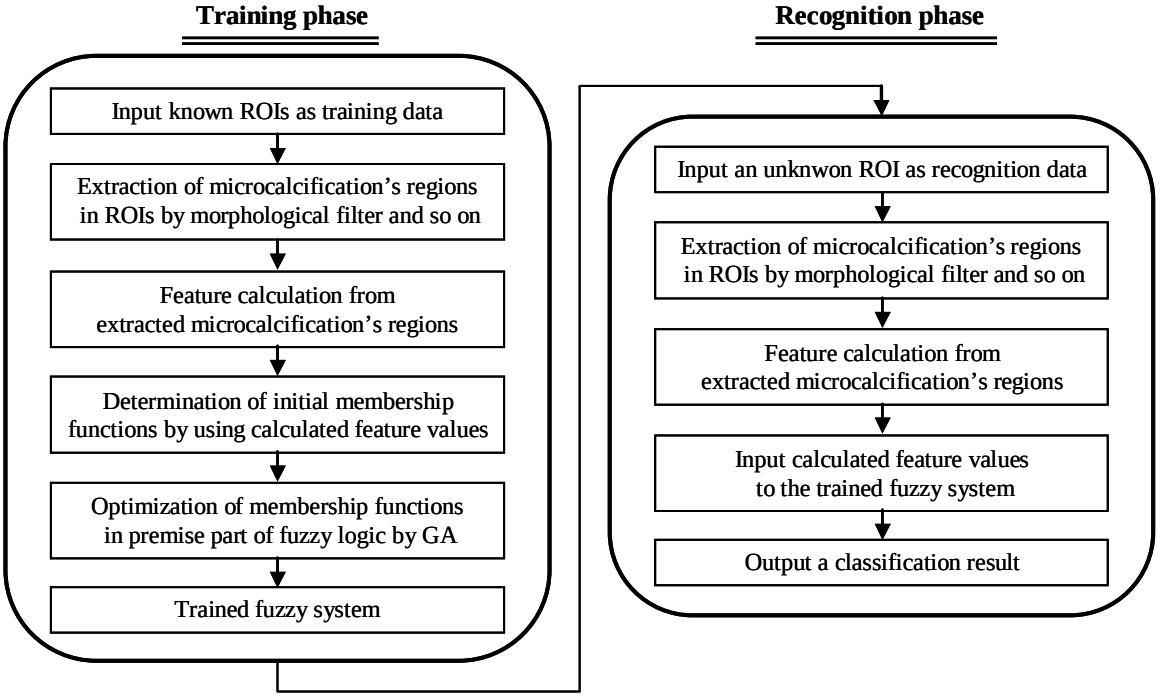

Fig.1 Procedural flowchart of our scheme

microcalcification's regions are extracted from ROIs by using morphological filter and so on [9]. Then, feature values including the total number, mean area, mean circularity and mean minimum distance are calculated from extracted microcalcification's regions in ROIs. These calculated feature values are used to derive initial membership functions in fuzzy logic. Then, GA is applied for optimizing membership functions in premise part of fuzzy logic. The trained fuzzy system is then used to classify unknown images in recognition phase. In recognition phase, microcalcification's regions are extracted from an unknown ROI, and feature values are calculated in the same manner as the training phase. A classification result, either benign or malignant is obtained by inputting the feature values to trained fuzzy system. Details of each process are described below.

2.2 Extraction of microcalcification's regions

The diagram for the extraction process of microcalcifications is shown in Fig.2. In this study, we use the mammographic database from the Mammographic Image Analysis Society (MIAS) in the United Kingdom. Each of the mammograms in the MIAS database was digitized at a spatial resolution of 50μm sampling distance with an 8-bit density resolution. Fig.3(a) shows an example of ROI with microcalcifications.

Median filter process is used to remove noise region in 50μm sampled images. Our contrast manipulation is indicated as follows:

$$F(i,j)=\begin{cases} 2f(i,j)-f_{\max} & f \geq \dfrac{f_{\max}}{2} \\ 0 & f < \dfrac{f_{\max}}{2} \end{cases} \tag{1}$$

where $f(i, j)$ is the pixel value at coordinate (i, j) in an original image and generally indicates an image in itself. f_{max} is the maximum value in density resolution of the image and is set at f_{max}=255 in this study. The purpose of this processing is to remove the unwanted structured background in the mammogram and to re-scale the gray values and, in turn, to make the subsequent processing more effective and functional. Fig.3(b) shows an image obtained by executing median filter process and contrast manipulation to Fig.3(a).

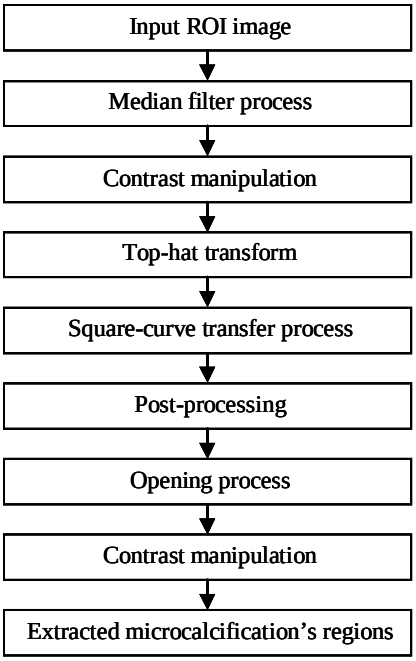

Fig.2 Diagram for the extraction process of microcalcification's regions

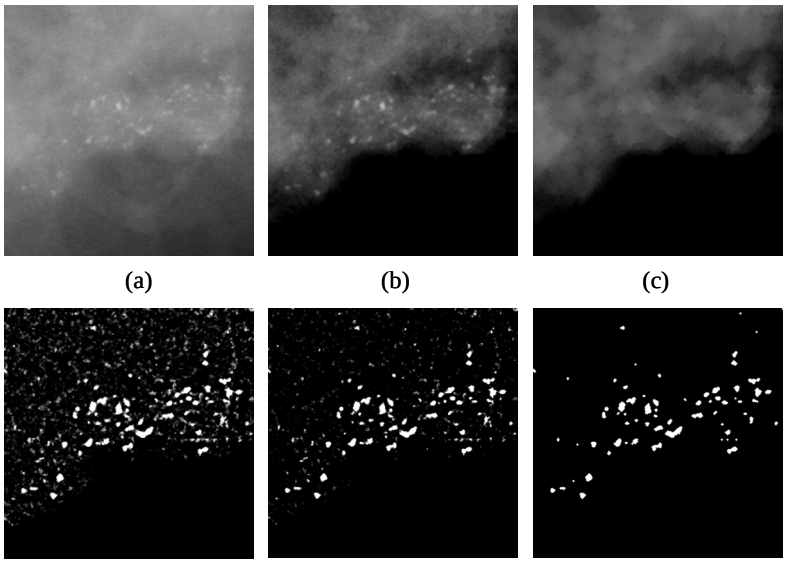

Fig.3 Original and processed images. (a) An ROI image in an original mammogram. (b) The image obtained by executing median filter and contrast manipulation to (a). (c) Opening processed image to (b). (d) The image after applying top-hat and after square-curve transformations to (c). (e) The image that applied post-processing to (d). (f) The image that executed opening and contrast manipulation and thresholding processes to (e).

Top-hat transformation appears as the following:

$$g(i, j) = F(i, j) - F(i, j)_{lowpassed} \tag{2}$$

where $F(i, j)$ is contrast-manipulated image obtained from equation (1), and $F(i, j)_{lowpassed}$ is the image obtained by applying a low-pass filter to $F(i, j)$. In this paper, mathematical morphology is used to get $F(i, j)_{lowpassed}$. For that, opening process using the cross-shaped structuring element of which diameter is eleven pixels applies to $F(i, j)$. Fig.3(c) is the image obtained by applying the opening process to Fig.3(b). Top-hat transformation used in this study is a subtraction process of the opening image from the original input image. It serves as a high-pass filter and has the property of enhancing potential microcalcification objects.

The pixel values in the image after performing top-hat transformation are remarkably low within a narrow range, and are not sufficient for visualization and for discrimination of each value. Square-curve operation shown as

$$G(i, j) = g(i, j)^2 \tag{3}$$

expands the pixel values for them. The image after applying top-hat and square-curve transformations to Fig.3(c) is shown in Fig.3(d).

After performing square-curve operation, there are many non-microcalcification objects such as blood vessels and noise among the clustered microcalcification candidates. Many of them are in a range of low pixel values. Those non-microcalcification objects can be buried by post-processing as the following:

$$y(i, j) = \frac{G(i, j)^2}{G_{\max}} \tag{4}$$

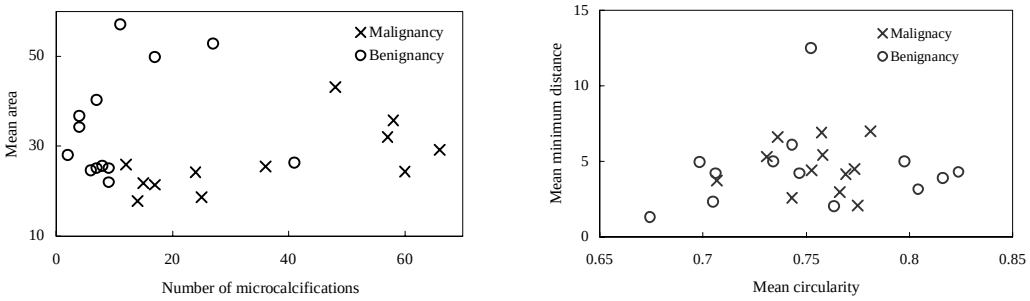

Fig.4 Distributions of calculated feature values. The left graph indicates the distribution of mean area versus the number of microcalcifications. The right graph indicates the distribution of mean minimum distance versus mean circularity.

where G_{max} is the maximum pixel value in $G(i, j)$. Fig.3(e) shows the image obtained by applying post-processing to Fig.3(d).

Several non-microcalcification objects remain at the present stage. Here, many of them are small objects with low pixel values. Therefore, opening process using the cross-shaped structuring element of which diameter is three pixels is employed to eliminate small objects. In addition, contrast manipulation is reused to eliminate low-density regions. Finally, regions of microcalcifications are extracted by thresholding process. Our final extraction result is shown in Fig.3(f).

2.3 Features Calculation

Four features including the microcalcification number(*Num*), mean area (*Area*), mean circularity (*Cir*) and mean minimum distance (*Clu*) are used to classify the clustered microcalcification in this study. The main reason for using these features is that radiologist's interpretation for classifying clustered microcalcifications would be based on their distribution, size, shape, and so on. These features are expressed as follows:

$$Num = n \tag{5}$$

$$Area = \frac{1}{n}\sum_{i=1}^{n} A_i \tag{6}$$

$$Cir = \frac{1}{n}\sum_{i=1}^{n} C_i \tag{7}$$

$$Dis = \frac{1}{n}\sum_{i=1}^{n} D_i \tag{8}$$

where n is the number of isolated candidate regions within an ROI image. A_i and C_i are the area of ith candidate and the circularity of the ith candidate, respectively. D_i is the distance from ith candidate to the nearest candidate. Fig.4 indicates distributions of features calculated from detected microcalcifications on mammograms in the MIAS database.

2.4 Classification by GA-FL

The GA-FL method using calculated feature values would discriminate between benignancy and malignancy of microcalcifications. The Gaussian-distributed membership functions (GDMFs) are employed in this study as premise-part membership functions for our fuzzy rule and given by

$$z(x) = \exp\left\{-\frac{1}{2}\left(\frac{x-\mu}{c\sigma}\right)^2\right\} \tag{9}$$

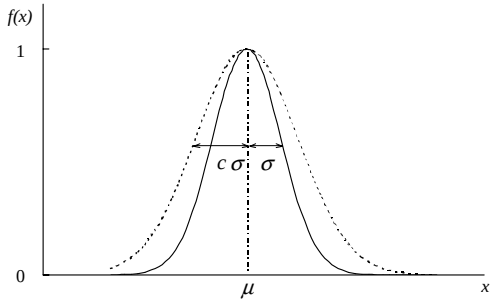

Fig. 5 Gaussian-distributed membership functions.

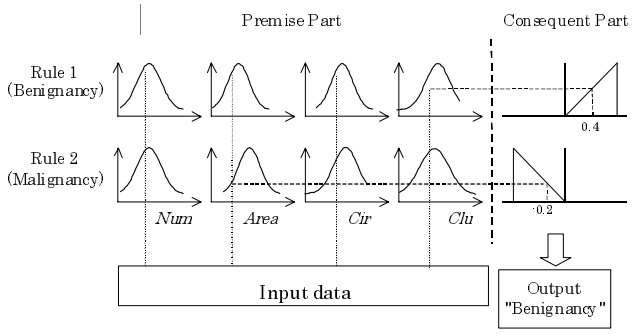

Fig. 6 Illustration of the fuzzy system used in this study.

C_{r1Nu}	C_{r1Are}	C_{r1Cir}	C_{r1Clu}	C_{r2Nu}	C_{r2Are}	C_{r2Cir}	C_{r2Clu}

Fig. 7 Chromosomes of an individual presented by two rules.

where μ and σ are the mean and the standard deviation of the distribution, respectively. c is a coefficient. Fig.5 shows an example of GDMF. The shape of GDMFs is determined from calculated feature values. μ and σ are equivalent to values of mean and standard deviation calculated by using feature values from a set of training images belonging to the same category. In this study, eight GDMFs are generated from four features (*Num, Area, Cir, Clu*) and two categories (Benignancy, Malignancy). Here, the shape of the consequent-part membership functions employed in this study is a right isosceles triangle with the maximum value of unity (normalized).

Fig.6 illustrates the fuzzy system that consists of eight premise-part membership functions and two consequent-part membership functions used in this study. Benignancy rule (Rule 1) and malignancy rule (Rule 2) are used in our fuzzy logic, and the MIN-MAX compositional rule of fuzzy inference is employed for defuzzification. The MIN-MAX compositional method is indicated as follows:

$$z_{r1} = \text{MIN}\ [\ |z_{r1}(Num)|, |z_{r1}(Area)|, |z_{r1}(Cir)|, |z_{r1}(Clu)|\ ]$$
$$z_{r2} = \text{MIN}\ [\ |z_{r2}(Num)|, |z_{r2}(Area)|, |z_{r2}(Cir)|, |z_{r2}(Clu)|\ ] \quad (10)$$

$$z_{r1 \cup r2} = \text{MAX}\ [\ z_{r1}, z_{r2}\ ] \quad (11)$$

$$\text{If } z_{r1 \cup r2} = z_{r1} \rightarrow \text{Benignancy}$$
$$\text{If } z_{r1 \cup r2} = z_{r2} \rightarrow \text{Malignancy} \quad (12)$$

where $z_{r1}(Num)$, $z_{r1}(Area)$, $z_{r1}(Cir)$ and $z_{r1}(Clu)$ are the respective GDMF values in rule 1 for the benign case, the same as that, $z_{r2}(Num)$, $z_{r2}(Area)$, $z_{r2}(Cir)$ and $z_{r2}(Clu)$ are the respective GDMF values in rule 2 for the malignant case. MIN and MAX are the operations that take the greater of two or more values and the lesser of two or more values, respectively. As a concrete example shown in Fig.6, since $z_{r1}=|z_{r1}(Clu)|=0.4$ (rule 1 for benign case) is greater than $z_{r2}=|z_{r2}(Area)|=0.2$ (rule 2 for malign case), the output of the fuzzy inference is "it is a benign clustered microcalcifications". Here, in the case of $z_{r1}= z_{r2}$, it is a "cannot decide" case. In this study, these cases are considered a failure and are regarded as misclassification.

Training for classification in this method is equivalent to determining μ, σ and c in GDMFs from training data. If the number of sample images is limited, the value of σ may not accurately reflect the characteristic of all images of the same category. Therefore in this study we use GA at training phase for determining the optimal membership function by varying the value of coefficient c.

An individual in our GA consists of eight chromosomes as shown in Fig.7. Each chromosome corresponds to a coefficient in GDMFs. For example, chromosome c_{r1Num} in Fig.7 indicates the coefficient c in GDMF that produced by the feature *Num* calculated from benign sample images. Each chromosome has 8-bit, and the range of c becomes $0.01 \leq c \leq 2.56$. We use selection, crossover and mutation as genetic operation. Procedure of GA used in this study is described as follows.

I. 200 individuals at the initial generation are generated randomly.
II. Fitness values are computed by using the fitness functions shown as follows:

$$fitness_1 = \frac{p-q}{p} \tag{13}$$

$$fitness_2 = \sum_{i=1}^{p} \left(z_{r1i} - z_{r2i}\right)^2 \tag{14}$$

where p and q refer to the numbers of learning data and misclassification. When $q = 0$, namely, all learning data are correctly classified during the training phase, then $fitness_1$=1.0. z_{r1i} and z_{r2i} represent the minimum GDMF values against ith sample image and are obtained from fuzzy rule 1 and rule 2, respectively. When the difference between z_{r1i} and z_{r2i} increases, the value of $fitness_2$ becomes greater.

III. Individuals are ranked according to the value of $fitness_1$. Those individuals having the same values of $fitness_1$ are further ranked according to the value of $fitness_2$.
IV. The last sixty low-ranked individuals are replaced by the same amount of new individuals obtained by employing crossover operation on the first sixty high-ranked individuals. The probability of mutation is 10% for each bit in the chromosome. Mutation operation is not implemented to the first twenty high-ranked individuals in a generation.
V. Steps II, III, and IV constitute one generation, and are repeated to fiftieth generation. The optimized coefficients are obtained from the individual having the highest fitness in the fiftieth generation.

The shapes of GDMFs are determined by the optimized coefficients been obtained at the training phase. Then unknown ROI images are classified by inputting their features into trained fuzzy system.

3. RESULTS AND DISCUSSION

Our methods were applied to twenty-five ROI images involving microcalcifications in the MIAS database. These ROI images consist of thirteen benign cases and twelve malignant cases. In the MIAS database, *x*, *y* coordinate of center of abnormality and approximate radius of circle enclosing the abnormality are recorded. We determined the sizes of ROIs according to them.

In training phase, ten benign cases and ten malignant cases were used as training data. The remaining five cases were used for classification as unknown images. All sets of their combinations were employed to obtain the result. Moreover, we obtained results using general GDMFs where the coefficients c was set at 1.0, namely, the GA was not used. The method without the GA is referred as to "FL" in this paper.

The results are shown in Table 1. In this table, denominators in parentheses are the total numbers of using one case for classification (Malignant: ${}_{11}C_{10} \times {}_{13}C_{10} = 11 \times 286 = 3146$, Benign: ${}_{12}C_{10} \times {}_{12}C_{10} = 66 \times 66 = 4356$), and numerators are the numbers of correct classifications for the case. Sensitivity and specificity are the probabilities of correct classifications for malignant and benign cases, respectively. The sensitivity rates for FL and GA-FL method were 66.3% and 84.8%, respectively. The specificity rates for FL and GA-FL method were 82.0% and 76.6%, respectively. Furthermore, overall accuracy is indicated as the probability of correct classifications for both categories. The accuracy of FL and GA-FL method were approximately 74.1% and 80.7%, respectively. When we only took into account those cases whose sensitivity and specificity were greater than 50%, the accuracy of FL and GA-FL methods were 72.0%(18/25) and 84.0%(21/25), respectively. The results indicate that the GA-FL method was more effective than FL.

The methods were also evaluated by ROC analysis. The classification accuracy was quantified by the area, Az, under the ROC curve. In the ROC evaluation, a conventional artificial neural network with back-propagation learning (BP-ANN) and an improved ANN based on GA to determine the weighting coefficients at ANN (GA-ANN) were also compared with FL and GA-FL. Structures of BP-ANN and GA-ANN are shown in Fig.8. The feature values calculated from an unknown ROI in Sec.2.3 were inputted input-layer at the both ANNs, as well as FL and GA-FL.

Fig.9 shows the ROC curves obtained by four classification methods (GA-FL, FL, BP-ANN, GA-ANN), and Table 2 shows the specificity and accuracy in the case that the sensitivity is 100 %. It is noted from the results that the GA-FL method shows the highest Az value (0.95) of ROC curve and the highest accuracy (88%). These results indicate usefulness of GA-FL. Here, in order to obtain the ROC curves, the following equations

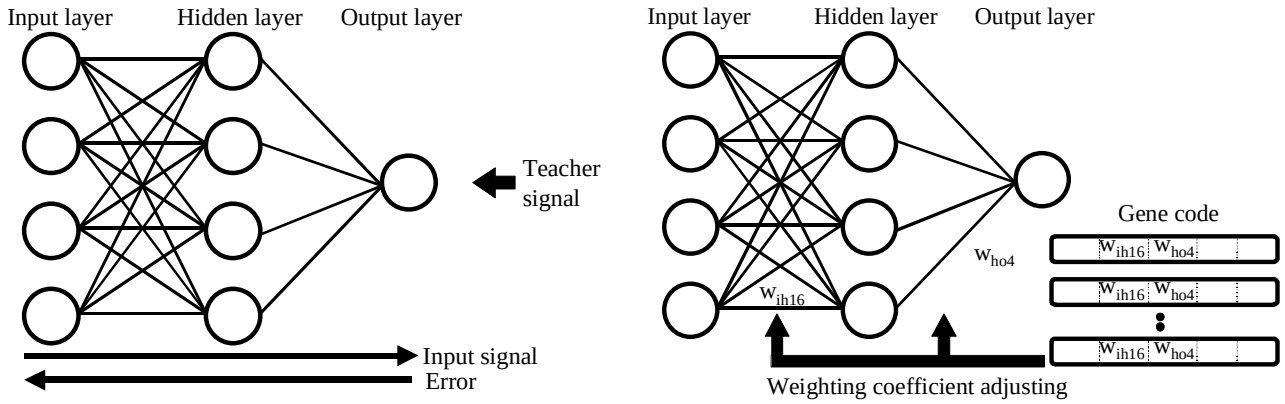

Fig.8 Structure of BP-ANN and GA-ANN used in this study. (a) Artificial neural network based on back-propagation. (b) Artificial neural network based on genetic algorithm

Table 1 Classification results utilizing FL and GA-FL.

		FL	GA-FL
	Case No.	Sensitivity	Sensitivity
Malignant cases	M1	100.0% (3146/3146)	100.0% (3146/3146)
	M2	37.8% (1189/3146)	90.0% (2831/3146)
	M3	42.8% (1345/3146)	61.7% (1942/3146)
	M4	100.0% (3146/3146)	100.0% (3146/3146)
	M5	0.5% (15/3146)	12.4% (389/3146)
	M6	100.0% (3146/3146)	100.0% (3146/3146)
	M7	44.5% (1399/3146)	97.5% (3068/3146)
	M8	61.1% (1921/3146)	81.4% (2560/3146)
	M9	100.0% (3146/3146)	100.0% (3146/3146)
	M10	33.7% (1059/3146)	74.4% (2342/3146)
	M11	100.0% (3146/3146)	100.0% (3146/3146)
	M12	75.4% (2373/3146)	99.8% (3140/3146)
	Total	66.3%(25051/37752)	84.8%(32002/37752)
	Case No.	Specificity	Specificity
Benign cases	B1	98.7% (4301/4356)	78.9% (3437/4356)
	B2	97.4% (4246/4356)	96.3% (4195/4356)
	B3	100.0% (4356/4356)	99.4% (4330/4356)
	B4	84.4% (3676/4356)	78.7% (3430/4356)
	B5	100.0% (4356/4356)	100.0% (4356/4356)
	B6	100.0% (4356/4356)	95.1% (4145/4356)
	B7	0.0% (0/4356)	4.5% (198/4356)
	B8	100.0% (4356/4356)	99.9% (4355/4356)
	B9	86.2% (3755/4356)	93.9% (4089/4356)
	B10	1.2% (54/4356)	10.0% (439/4356)
	B11	100.0% (4356/4356)	100.0% (4356/4356)
	B12	100.0% (4356/4356)	100.0% (4356/4356)
	B13	97.4% (4241/4356)	38.3% (1169/4356)
	Total	82.0%(46409/56628)	76.6%(43355/56628)

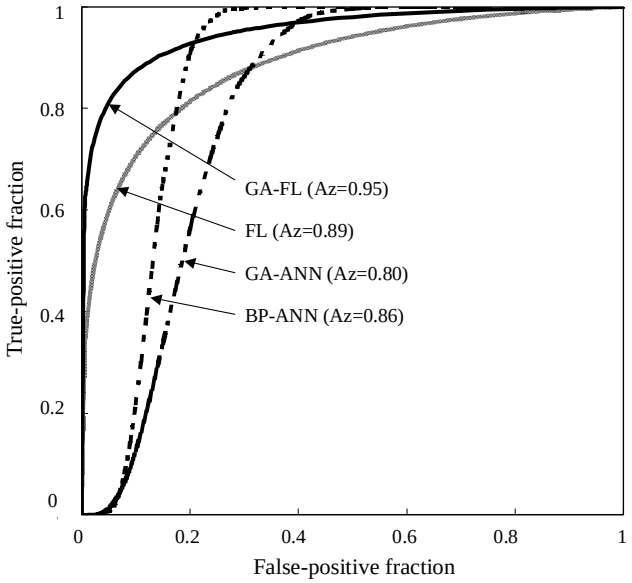

Fig.9 ROC curves obtained from each classification results.

Table 2 Classification results utilizing BP-ANN, GA-ANN, FL and GA-F when sensitivity is 100 %.

	Sensitivity	Specificity	Accuracy
BP-ANN	100%	69%	85%
GA-ANN	100%	54%	77%
FL	100%	31%	65%
GA-FL	100%	77%	88%

$$z_{r1 \cup r2} = z_{r2} - z_{r1} \tag{15}$$

If $z_{r1 \cup r2} < th$ → Benignancy
If $z_{r1 \cup r2} \geq th$ → Malignancy (16)

were substituted for equation (11) and (12). *th* is a threshold value. $z_{r1 \cup r2}$ has a range of -1.0 to 1.0, and is close to 1.0 if being malignancy case.

The results implied the potential usefulness of our proposed GA-FL method. However, to improve the classification performance, it is still necessary to investigate the detection performance of microcalcifications and to reconsider the adequate features and to increase sample images.

4. CONCLUSION

In this paper, we have described a new scheme for automated classification of mirocalcifications on mammograms using fuzzy logic that applied genetic algorithm to optimize the premise-part membership functions (GA-FL). In this scheme, our extraction method using morphology filter for microcalcification's regions was performed. The proposed GA-FL method was applied to mammographic micorcalcifications in the MIAS database. As the results, the accuracy of classification was 88% (Sensitivity 100%, Specificity 77%), and Az value of the ROC curve was 0.95. Moreover, GA-FL was compared with conventional fuzzy-logic method (FL) and two ANN methods (BP-ANN and GA-ANN). The results show that GA-FL had the highest accuracy and Az value of ROC curve among the four classification methods. Future work increasing sample images for further feasibility test on the proposed method is needed.

ACKNOWLEDGMENT

This work was supported in part by a Grant-In-Aid for Scientific Research (Intelligent Assistance for Diagnosis of Multi-dimensional Medical Images) from the Ministry of Education, Culture, Sports, Science and Technology.

REFERENCES

1. Y. C. Wu, M. T. Freedman, A. Hasegawa, R. A. Zuurbier, S. C. Lo and S. K. Mun, "Classification of microcalcifications in radiographs of pathologic specimens for the diagnosis of breast cancer", *Academic Radiology*, **2**(3), 1995, 199-204.
2. H. P. Chan, B. Sahiner, N. Petrick, M. A. Helvie, K. L. Lam, D. D. Adler and M. M. Goodsitt, "Computerized classification of malignant and benign microcalcifications on mammograms: Texture analysis using an artificial neural network", Phys. Med. Biol., **42**(3), 1997, 549-567.
3. T. Hara, A. Yamada, H. Fujita, T. Iwase and T. Endo, "Automated classification of mammographic microcalcifications by using artificial neural network an ACR BI-RADS criteria", *Proc. of SPIE,* **4322**, 1783-1787, San Diego, USA, 2001.
4. H. P. Chan, B. Sahiner, K. L. Lam, N. Petrick, M. A. Helvie, M. M. Goodsitt and D. D. Adler, "Computerized analysis of mammographic maicrocalcifications in morphological and texture feature spaces", *Medical Physics*, **25**(10), 1998, 2007-2019.
5. Y. Lee, D.Y. Tsai and M. Sekiya, "Computerized Classification of Clustered Microcalcifications on Mammograms", *Proc. of the Second IASTED International Conference on Visualization, Imaging, and Imaging Processing*, 406-411, Malaga, Spain, 2002.
6. T. Katafuchi, H. Fujita, K. Asai & T. Uehara, "Development of a computer-aided diagnosis system using fuzzy inference in 201T1C1 exercise myocardial scintigraphy", *Japanese Journal of Radiological Technology*, **56**(3), 377-383, 2000.
7. D.Y. Tsai and Y. Lee, "Fuzzy Reasoning Based Computer-Aided Diagnosis for Automated Discrimination of Myocardial Heart Disease from Ultrasonic Images", *Electronics and Communication in Japan; Part 3: FUNDAMENTAL ELECTRONIC SCIENCE*, **85**(11), 1-8 2002.
8. D.Y. Tsai, Y. Lee, M. Sekiya, M. Ohkubo, K. Kojima, and I. Yamada, "An Integrated Fuzzy-GA-Based CAD System for Disease Discriminations", *Proc. of the IASTED International Conference on Biomedical Engineering*, 166-171, Salzburg, Austria, 2003.
9. D. Y. Tsai, M. Sekiya, Y. Lee, Y. Yamazaki, M. Ohkubo, K. Kojima, & I. Yamada, "A morphology -based method for automated detection of clustered microcalcifications", *Proc. of IASTED International Conference Signal Processing, Pattern Recognition, and Applications (SPPRA2001)*, 159-162, Rhodes, Greece, 2001.

*lee@clg.niigata-u.ac.jp; phone +81-25-227-0957; fax +81-25-227-0749